Mapping and monitoring subtle ground deformation in Sindos, Greece, with high precision digital leveling

Panagiotis Kalaitzis[1,*], Antonios Mouratidis[2,3], Polyvios Vladenidis[2,3], Dimitrios Ampatzidis[4], Georgios Moshopoulos[5], Christos Domakinis[3], Zoe Pantazopoulou[2,3], Georgia Karadimou[2,3], Triantafyllia-Maria Perivolioti[2,3], Dimitrios Terzopoulos[6], Evaggelos Giataganas[3], Michael Foumelis[2,3], Nikolaos Soulakellis[1], Konstantinos-Vasileios Katsampalos[5]

[1] Department of Geography, Faculty of Social Sciences, University of the Aegean, Greece
[2] Center for Interdisciplinary Research and Innovation (CIRI-AUTH), Balkan Center, Greece
[3] Aristotle University of Thessaloniki, Department of Physical and Environmental Geography, Greece
[4] International Hellenic University, Department of Surveying and Geoinformatics Engineers, Greece
[5] Aristotle University of Thessaloniki, Department of Geodesy and Surveying, Greece
[6] Aristotle University of Thessaloniki, School of Medicine, Greece
* Corresponding author: p.kalaitzis@geo.aegean.gr

ABSTRACT

Several studies have focused on the ground displacement phenomena in the broader area of the Thessaloniki Plain, Greece. Although there is a general consensus on the diachronic occurrence of subsidence, there have been recent studies that also report considerable uplifts. In order to resolve some of these ambiguities and to further study and monitor the area, new, high-accuracy leveling measurements were conducted during 2018–2020 in the vicinity of the town of Sindos. Findings indicate a total vertical displacement of up to about −15 mm, whereas the continuation of a clear overall subsidence tendency rather than uplift has been verified.

KEYWORDS

subsidence; uplift; levelling; digital levelling; mapping; Sindos; Thessaloniki; Greece

Received: 14 September 2022
Accepted: 19 December 2022
Published online: 20 February 2023

Kalaitzis, P., Mouratidis, A., Vladenidis, P., Ampatzidis, D., Moshopoulos, G., Domakinis, C., Pantazopoulou, Z., Karadimou, G., Perivolioti, T.-M., Terzopoulos, D., Giataganas, E., Foumelis, M., Soulakellis, N., Katsampalos, K.-V. (2023):
Mapping and monitoring subtle ground deformation in Sindos, Greece, with high precision digital leveling
AUC Geographica 58(1), 3–17
https://doi.org/10.14712/23361980.2023.1

1. Introduction

Subsidence is a type of geological hazard that is generally subtle and imperceptible in real-time, typically necessitating at least a couple of years of observations to identify. Nevertheless, the consequent disaster may be particularly catastrophic, especially in the presence of certain conditions, e.g., when occurring in low-lying coastal urban centers, populated deltas or coastal protected areas. One of the factors contributing to subsidence is the uncontrolled pumping of water and oil from underground, which particularly escalated in the twentieth century and has led to significant economic and cultural losses (Bolt et al. 1977).

Climate change and associated sea level rise is expected to considerably aggravate the impact of such coastal subsidence geohazards in the years to come (Elias et al. 2020). This is due to the fact that the combined climate-induced sea-level rise and vertical land movements, including natural and human-induced subsidence in sedimentary lowlands, have a higher impact (up to four times faster), in terms of average relative sea-level rise, over coastal areas (Nicholls et al. 2021).

Such an example is the broader area of the Thessaloniki Plain, northern Greece, where several studies have detected vertical ground displacements since the 1960s. Especially at the eastern edge of the Plain, in the vicinity of the coastal front, the Sindos–Kalochori wider area has been the most interesting one and hence the focus of the majority of studies. The comparison between past leveling and Global Navigation Satellite System (GNSS) data indicates that sections of the plain of Thessaloniki, especially those close to the modern Galikos and Axios river mouths, have undergone subsidence of up to 4 m in the last 50 years (Stiros 2001; Psimoulis et al. 2007). Most researchers highlight the over-exploitation of groundwater as the main cause of subsidence phenomena (Hadzinakos, Rozos, and Apostolidis 1990; Andronopoulos, Rozos, and Hadzinakos 1991). However, a number of experts suggest alternative interpretations, such as the compaction of the shallow sediment layers and the synsedimentary deformation of the delta (Stiros 2001), the coastal erosion and the rise of sea level (Doukakis 2005), the combination of natural and anthropogenic factors (Psimoulis et al. 2007) and the compaction of unconsolidated silt-clay deposits near coastline (Dimopoulos, Stournaras, and Pavlopoulos 2005). Although groundwater exploitation in the area started in the early 1960s in order to facilitate industrial development, subsidence was not noticed until 1965, indirectly, manifesting as progressive marine water inflow (Raspini et al. 2014). In 1969, during a period of intensive rainfall, seawater reached the southern houses of the village (Mouratidis et al. 2010). Previous studies have exploited the archive of the ERS satellite Synthetic Aperture Radar (SAR) data (1991–2000), for implementing conventional and Persistent Scatterer (PS) SAR Interferometry (InSAR) measurements, as well as the equivalent part of the Envisat Advanced SAR (ASAR) data (2002–2010) for standard and elaborated InSAR processing (Raucoules et al. 2008; Costantini et al. 2016; Mouratidis 2017). According to these studies, the estimated subsidence rate in the vicinity of Sindos-Kalohori ranges between about 2 and 5 cm/yr (Costantini et al. 2016).

Nevertheless, some authors (Svigkas et al. 2016) contradict part of the aforementioned results and highlight a significant uplift signal in the area, suggesting a rebound phenomenon. More specifically, from 2003 to 2010, an uplift tendency of up to +12 mm/yr was reported in the Sindos-Kalohori area, as opposed to the 1992–2000 subsidence of more than 20 mm/yr. Regarding the spatial distribution of the uplifting pattern, the pixels in and around Sindos with uplift values close to the maximum are only slightly fewer than those recorded in the adjacent area of Kalochori (Svigkas et al. 2016), indicating a relatively isotropic phenomenon.

The most recent deformation measurements in the area of Sindos come from InSAR studies, in the era of Sentinel-1 SAR mission. These indicate subsidence rates of about 10 mm/yr for the period 2014–2019 (Elias et al. 2020) and 14 mm/yr during 2015–2019 (Svigkas et al. 2020).

In this context, the purpose of this study is twofold; a) to resolve any ambiguities regarding the current (2018–2020) status of Sindos in terms of vertical ground deformation (subsidence or uplift), by applying, for the first time in this area, sub-millimeter precision methods, and b) to establish a high precision monitoring network, in order to ensure the continuity of monitoring efforts with reliable in-situ observations in the near future either as a standalone approach or as a complementary (ground truth, calibration and validation data) to other monitoring/observational Remote Sensing methods (e.g. InSAR) and corresponding networks (e.g. Global Navigation Satellite Systems/GNSS).

2. Study Area

The study area is the broader region of the town of Sindos or Sinthos (older name, Tekeli) (Fig. 2). Sindos (40°40′0″ N 22°48′0″ E) lies about 14 km NW of the city of Thessaloniki, northern Greece, and belongs to the Municipality of Delta. It is an almost flat, low-elevation (5–10 m) region and covers an area of about 5 km^2, in the vicinity of four major rivers (Gallikos, Axios, Loudias, Aliakmonas). According to the 2011 census, there are 9289 inhabitants in the area, with agricultural activities being the primary occupation.

During the last decades, the area was gradually transformed into a suburban-industrial zone due to the expansion of the nearby city of Thessaloniki. In

1965, Sindos was designated as the Industrial Park of Thessaloniki. Nowadays, more than 300, mostly small, factories are operating in the area. In Sindos, there are also other important facilities besides those that define it as the Industrial Zone of Thessaloniki. These include the facilities of the International Hellenic University (IHU) and, in the wider area, the facilities of the city's water supply and sewerage company (EYATH) and biological wastewater treatment.

From a geological point of view, Sindos consists of Holocene deposits which are characterized as coastal deposits with fossils of gastropods. These deposits are unconsolidated to partly consolidated marine-lacustrine sediments, filling a NW–SE oriented tectonic graben, consisting mainly of sand and black silty clays (Rozos, Apostolidis, and Xatzinakos 2004; Hadzinakos, Rozos, and Apostolidis 1990). The

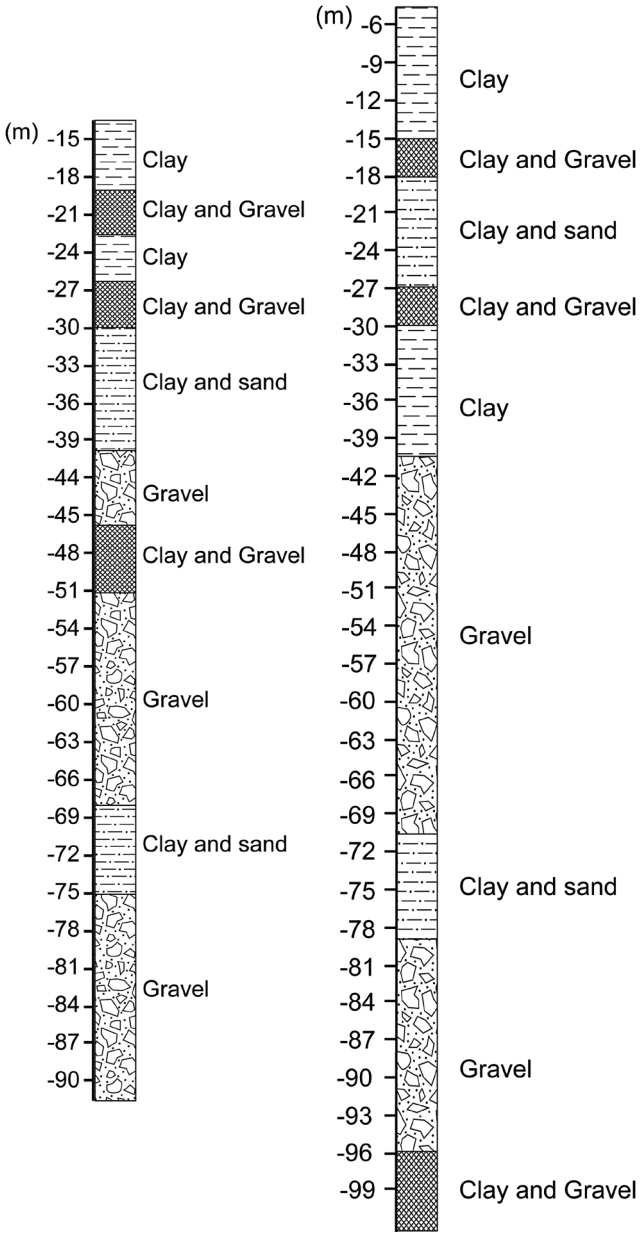

Fig. 1 Two recent, indicative stratigraphic columns of the broader area of Sindos (Tsourlos et al. 2007).

Neogene basement, buried by a 300–400 m thick sequence of Quaternary deposits, is represented by sandstones, red clays and outcrops in the north and in the north-east border of the area of interest (Raspini et al. 2014). The materials that are found are mainly sands, red clays with calcareous compositions, and conglomerates (Tsourlos et al. 2007) (Fig. 1). The existence of these elements in the area indicates that the plain of Thessaloniki probably was part of the Thermaikos gulf, and, at some point, Sindos used to be a coastal area (Ghilardi et al. 2008). Generally, the area is comprised of recent unconsolidated material, which form on multiple aquifer systems. Three main aquifers can be identified: one phreatic and two deep confined aquifers. The water level within these deposits was at an average depth of about 10–15 m below ground surface. The groundwater table is below sea level. The mean hydraulic conductivity was estimated to be $k = 6.5 \times 10^{-3} - 1.5 \times 10^{-2}$ m/min, Transmissivity (T) = 0.55–0.94 m^2/min, Storage coefficient (S) = 10^{-3} (Tsourlos et al. 2007). Further information about individual boreholes in the area can be found in additional studies (Mattas, Voudouris, and Panagopoulos 2014). According to climate data from the Meteorological station of Thessaloniki (40°03′ N, 22°58′ E) the mean annual temperature is 15.8 °C and the mean annual precipitation is 451.7 mm (Pateli et al. 2002).

The reasons for the occurrence of subsidence lie in both natural, as well as anthropogenic processes, related to the compaction of sediments and over-exploitation of aquifers (Astaras and Sotiriadis 1988).

3. Methodology

3.1 Method and Instrumentation

The most common methods for measuring subsidence and studying its spatial distribution are GNSS, InSAR and leveling, each of which has its advantages and drawbacks, while the combination of multiple techniques bears the potential of more enhanced results (Blasco et al. 2019; Del Soldato et al. 2018; Argyrakis et al. 2020).

In the spatial domain, spirit leveling, GNSS and extensometer measurements are relatively sparse, as these measurements can only be taken at a comparably restricted number of locations. InSAR measurements on the other hand are spatially dense, with their resolution (and thus density) depending on the pixel size of the SAR data used. Nevertheless, high-precision (mm) InSAR methods require, at the time of this writing, a few months of SAR observations, in order to accumulate a sufficient amount of data. Additionally, these InSAR results are provided in the form of a deformation rate (mm/yr), assuming a linear evolution of the phenomenon. Thus, potential variations within the considered time period may be

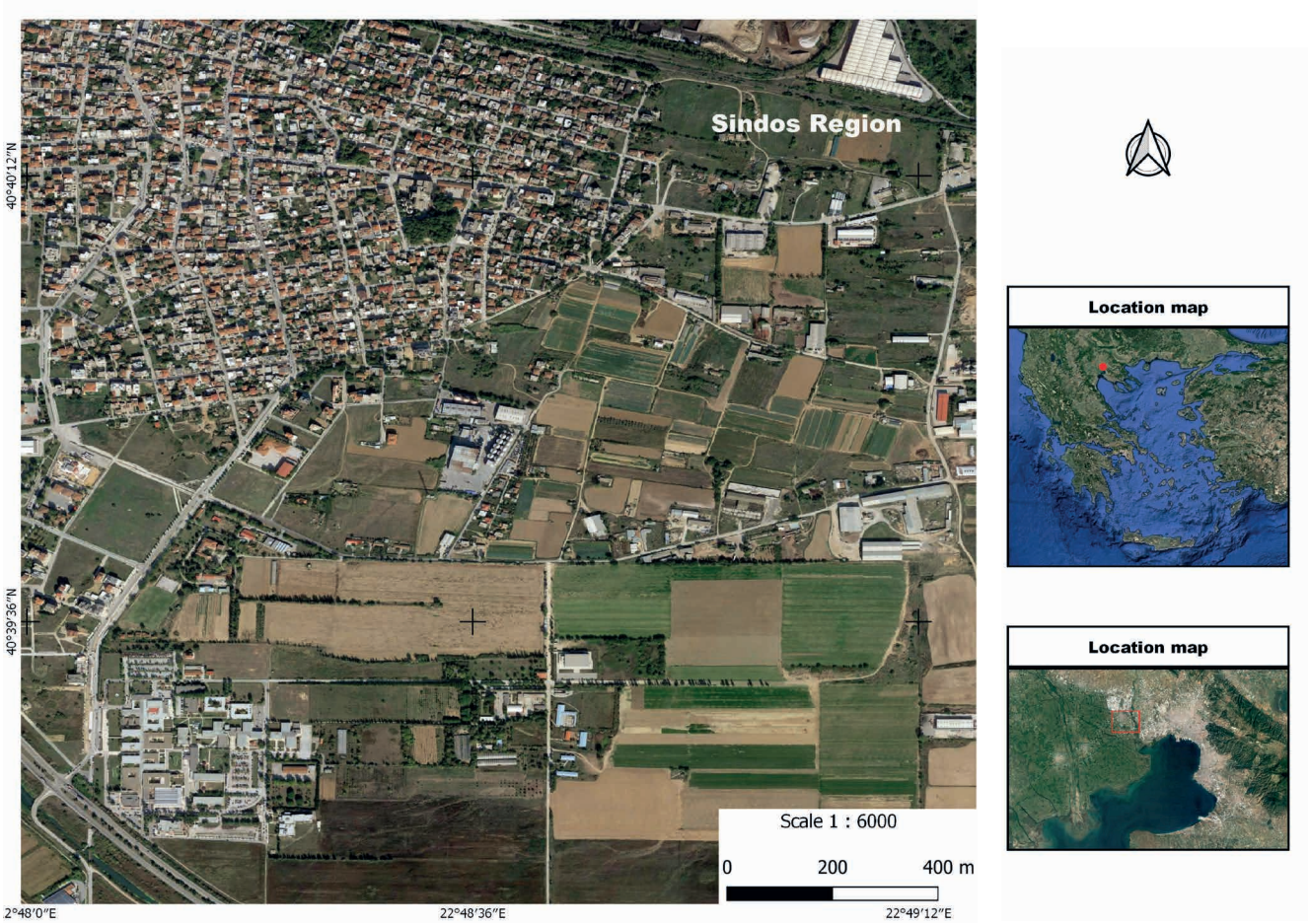

Fig. 2 Overview of the study area (Background source: Google™).

cancelled out, while a certain degree of in-situ validation is also typically desirable.

The frequency of measurement highly depends on the study objectives, the measurement methods, the available manpower and the expected order of magnitude of the subsidence rates. Very slow subsidence rates may not be possible to capture by GNSS measurements over a period of several years, due to the low signal-to-noise ratio (enough subsidence needs to occur between measurements to exceed the expected measurement error). In this case, a more accurate method, such as spirit leveling, may be necessary, in order to obtain meaningful results within a reasonable timeframe.

Overall, the most precise measurements are made using spirit-leveling surveys and extensometers. High precision leveling has been efficiently used e.g. for the purposes of monitoring crustal vertical deformation (Hao et al. 2014; Chen et al. 2021), post-glacial land uplift (Kall, Oja, and Tänavsuu 2014), inter-seismic deformation (Amighpey, Voosoghi, and Arabi 2016), in hydropower projects (Guanming et al. 2019), but also for calibrating or validating satellite-based land subsidence rates (Fryksten and Nilfouroushan 2019; Hung et al. 2018; USGS n.d.).

Taking into account these considerations and given the verified low deformation rates (whether subsidence or uplift) during the last two decades in the Sindos area (Svigkas et al. 2020; 2016; Elias et al. 2020), the method selected, in order to fulfil the objectives of this study, was spirit leveling.

The equipment used for the measurements was Leica DNA03™, which is a high precision digital level, with a nominal accuracy (Standard deviation per km double run) of ± 0.3 mm with invar staff or ± 1 mm with standard staff.

Fig. 3 The equipment, Leica DNA03™ and the staff (Professional 3000 series), that was used for the leveling measurements.

3.2 Network Design

The leveling network consisted of eleven points that cover the study area. The mean, maximum and total distance between all points is about 500 m,

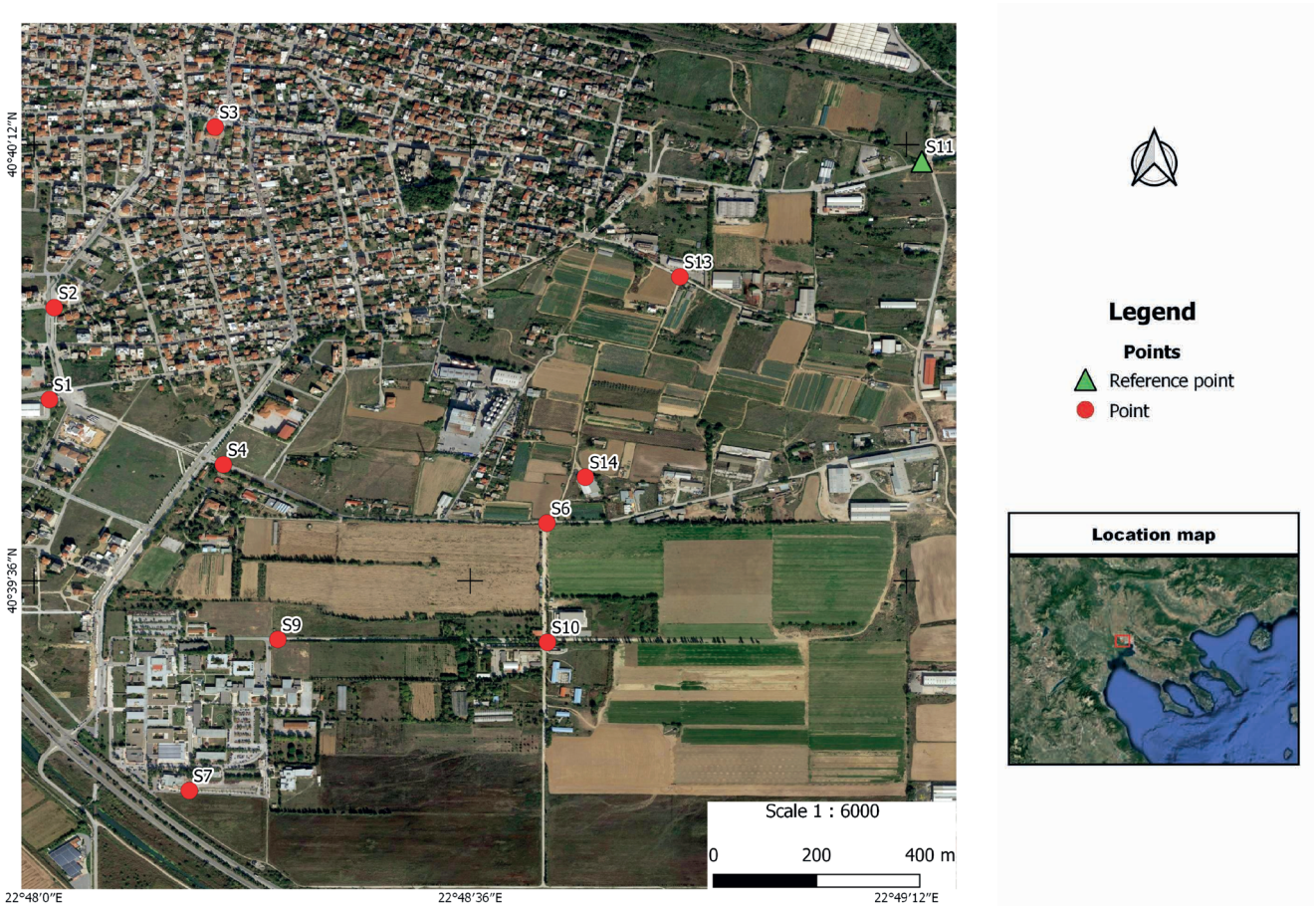

Fig. 4 The leveling network used in this study, including ten fixed points and the considered stable reference point (red dots and green triangle respectively).

1.4 km and 5 km respectively. The location of each point was carefully selected according to the following criteria:

- Coverage (including the approx. N-S and E-W boundaries of the study area).
- Accessibility.
- Minimum interference with public and (predominantly) private property.
- Conspicuity and durability.
- One of these points should be as far from the affected area as possible (given local conditions, total distance for leveling and safety regulations), in order to serve as the reference ("stable") point for all measurements.

Note that three additional points (namely S5, S8 and S12) were originally established in 2018, but

Tab. 1 The exact location and design details of each point of the established network are listed on the table below.

Point No.	Point Name	Lat	Lon	Description
1	S1	40.6641	22.8003	The westernmost point in the study area. It is located near the municipal gym of Sindos.
2	S2	40.6662	22.8004	Point facilitating the transition towards the center of Sindos. It is located near the 3rd elementary school.
3	S3	40.6704	22.8041	The northernmost point in the study area, located on the main square of Sindos Town.
4	S4	40.6626	22.8043	Located on the road, at the main entrance of Sindos.
5	S6	40.6613	22.8117	Point located at approximately the center of the study area.
6	S7	40.6551	22.8035	The southernmost point, located on the pavement, in the International Hellenic University (IHU) campus.
7	S9	40.6586	22.8055	Second point located in the main IHU campus.
8	S10	40.6585	22.8117	Point located on the road, near the IHU agricultural fields.
9	S11	40.6696	22.8203	The reference point, located in the NE boundary of the study area.
10	S13	40.6669	22.8148	Point located on the road, facilitating the transition towards the central point, S6.
11	S14	40.6623	22.8126	Point located on the road, facilitating the transition towards the central point, S6.

were eventually lost (destroyed due to external factors) by 2020.

Based on the diachronic InSAR measurements and other previous results (Mouratidis, Costantini, and Votsis 2011; Mouratidis et al. 2010; Raucoules et al. 2008; Costantini et al. 2016; Raspini et al. 2014; Svigkas et al. 2016) in the study area, the vertical displacement tends to zero towards the NE. At this point, it ought to be taken into account that Sindos is an industrial area, including highways, bridges, intense truck traffic and other heavy vehicles, combined with an inherent poor town/road planning. These create overall adverse field work conditions and imposes constrains related to safety of the people involved in the measurements. Given also the practical limitations in terms of distance that can be covered with leveling, point S11 (Fig. 4) was rendered as the best choice for a reference point. In fact, as indicated in some of the high-resolution results (Svigkas et al. 2016), the selected reference point is (marginally) located inside the stable area. It also has to be noted that these results refer to the period 1993–2000, when the subsidence rates were considerably higher (more than double) than in the post-millennial period. Therefore, S11 was already stable as early as 2000, when the overall subsidence rates in the broader area were much larger.

In order to secure the network as much as possible, but also to establish a reference for future studies (when significant deformation is expected to have accumulated), static, approximately hourly, GNSS measurements were conducted at each of the points. To this end, geodetic, dual (L1, L2) frequency Topcon Hiper pro™ GNSS receivers were used, at a sampling rate of 30 sec and with a cut-off angle of 5°. These measurements were coupled with equivalent, simultaneous GNSS observations outside the study area, at a distance well below 20 km (in Pylaia, Thessaloniki).

3.3 Data Collection and Processing

Spirit leveling was then performed in a double-run mode, between all consecutive network points, with several loops in-between (Fig. 6), in order to minimize blunders. Backsights and foresights were approximately equal in distance, ranging between 40–50 m, with an average of 42 m. The measurements were also carried out during similar periods of the year for three years (i.e., May–June 2018, 2019 and 2020), so as to avoid seasonality-related effects as much as possible.

As a first level of quality assurance, each double-run measurement that did not satisfy a closure of ±0.5 mm was executed again, until the desired threshold was achieved. The final height difference between two points was then calculated as the mean value

Fig. 5 Approximate distance between network of points and GNSS stable station at Pylaia.

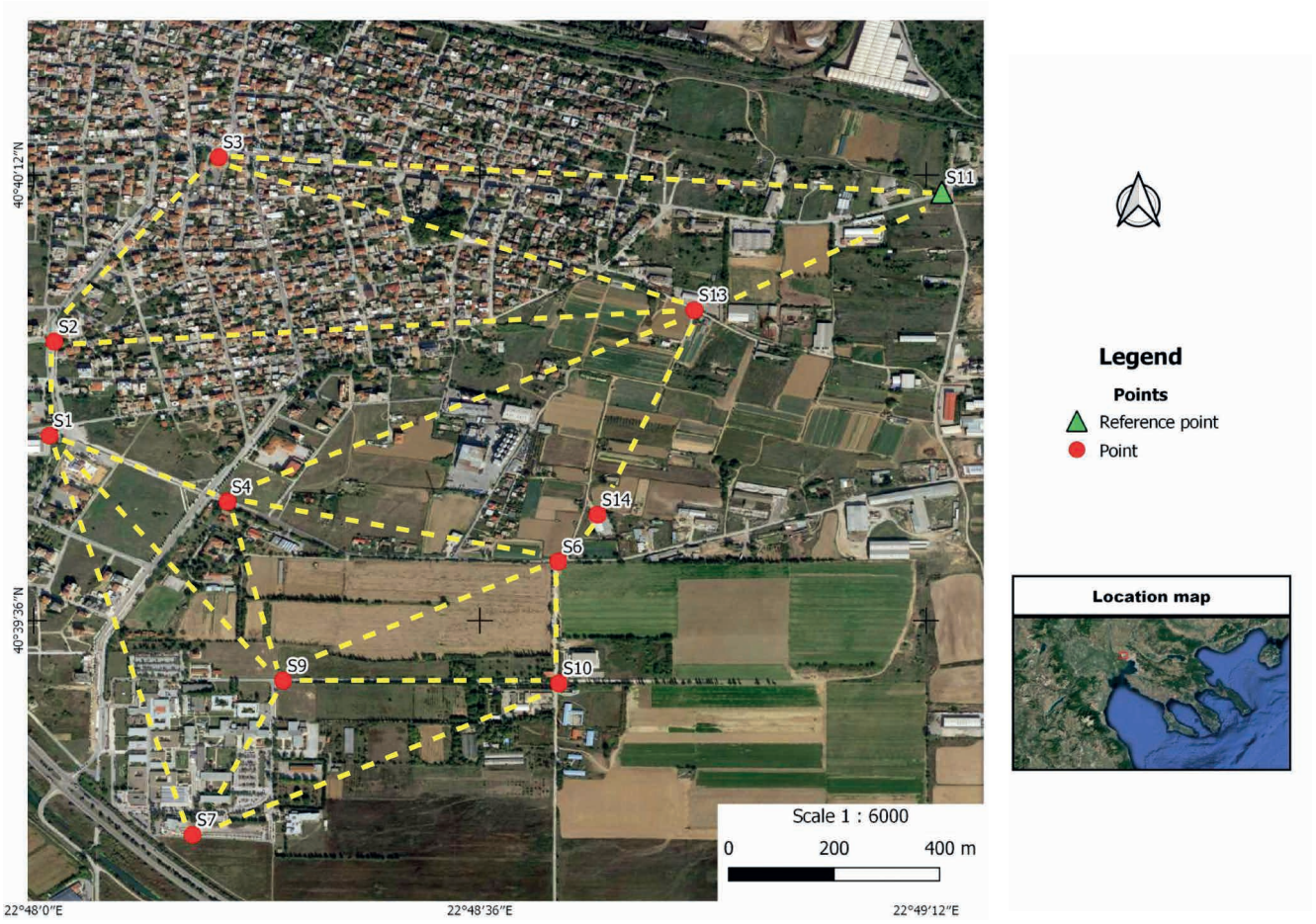

Fig. 6 Complete sketch of the leveling network, including the loops performed on an annual basis from 2018 to 2020.

between the double run measurements, fulfilling the threshold. To further ensure robustness against blunders, as well as to enable residual error redistribution, the leveling network was designed with multiple loops. An empirical threshold of the loop closure was set; If the loop closure was larger than ±15 mm, the double-run leveling for this particular loop was repeated.

Tab. 2 Summary of the conducted leveling main characteristics.

Vertical Deformation (mm)			
Point	**June 2018 – June 2019**	**June 2019 – June 2020**	**June 2018 – June 2020**
S1	−9.3 ± 0.73	−0.6 ± 0.75	−9.9 ± 0.74
S2	−7.3 ± 0.73	−3.4 ± 0.74	−10.7 ± 0.74
S3	−5.3 ± 0.71	−2.9 ± 0.71	−8.2 ± 0.72
S4	−8.8 ± 0.72	−0.4 ± 0.7	−9.2 ± 0.71
S6	−8.5 ± 0.69	0.7 ± 0.69	−7.8 ± 0.68
S7	−15.1 ± 0.75	0.8 ± 0.75	−14.3 ± 0.75
S9	−11.6 ± 0.71	0.7 ± 0.71	−10.9 ± 0.7
S10	−14.4 ± 0.71	−0.6 ± 0.71	−15.0 ± 0.71
S11	Reference Point		
S13	−2.9 ± 0.58	3.2 ± 0.57	0.3 ± 0.58
S14	−5.5 ± 0.67	3.0 ± 0.68	−2.5 ± 0.67

All of the collected leveling data were imported in a Geographical Information System (GIS) environment, specifically QGIS. For this process it was necessary to decode and transfer the data from the digital level to a readable PC format, as well as to pre-process them, in order to be fully and properly readable by the GIS software. The next step was to calculate the relative height difference of each point in relation to the reference point. Finally, the values calculated from the three datasets were subtracted (2019–2018, 2020–2019, 2020–2018), with the purpose of determining the relative vertical displacement of every point, always in relation to the reference point.

3.4 Quality Analysis of the established Vertical Network

The vertical network was solved by applying least squares adjustment for three successive years (2018, 2019, 2020), using the DeRos software (Dermanis and Rossikopoulos 1981). Specific rigorous criteria (double run and loop–closure controls, respectively) for the elimination of potential blunders were applied. The solution was based on minimum constraints (Koch 1999), fixing the reference point (which is laid far away from the area of interest). The outlier identification and rejection were realized by the application of the data-snooping method (Dermanis and

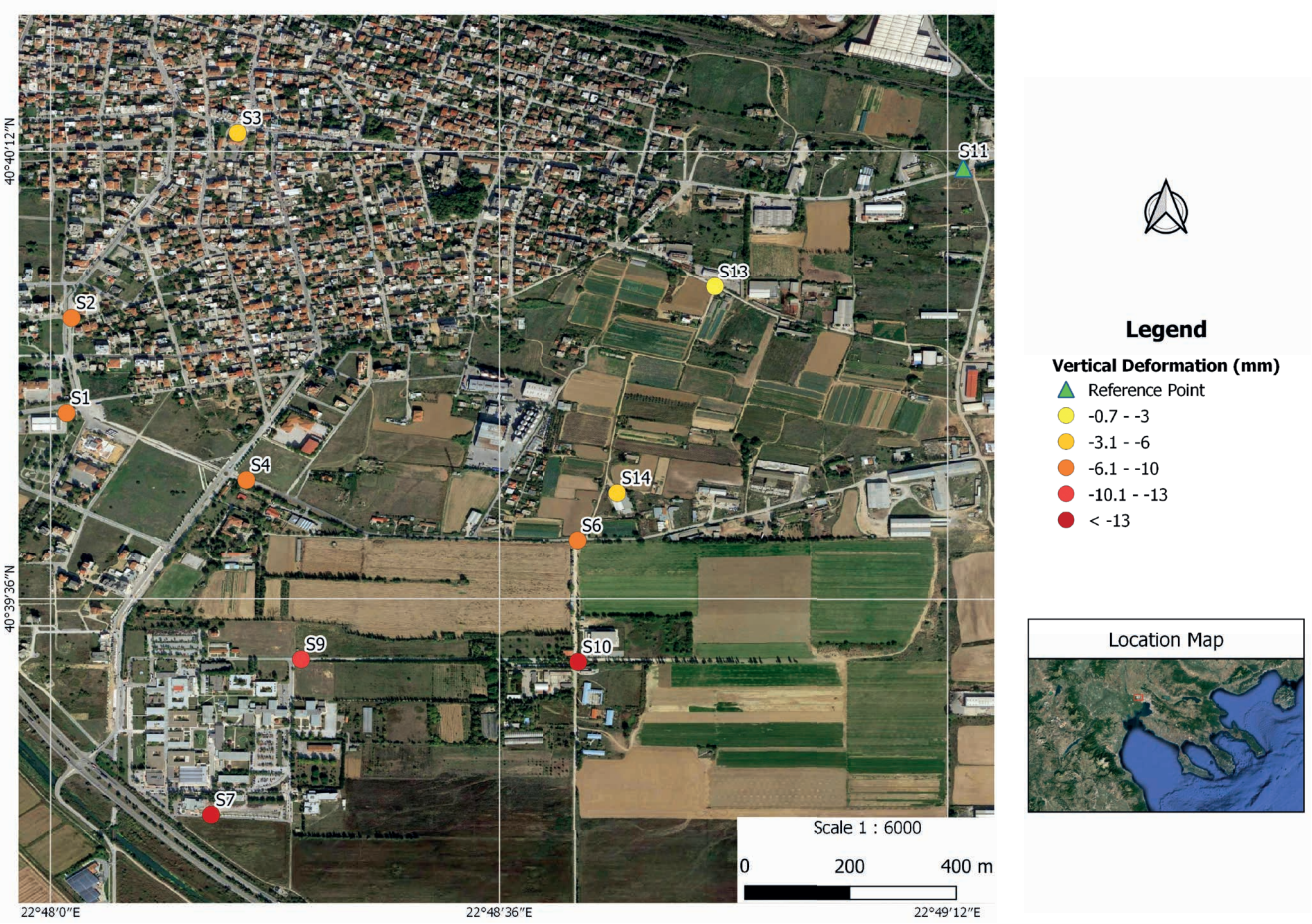

Fig. 7 Vertical displacements between June 2018 and June 2019.

Fotiou 1992; Rossikopoulos 1999). The t-test (Student's t-test) was implemented with a 95% level of confidence.

After performing adjustment on an annual basis, the estimation of the heights and their associated accuracies were obtained, for the respective years. In order to assess the significance of the estimated vertical displacement the following criterion was applied, pointwise (Dermanis 1986):

$$\frac{h_i^k - h_i^j}{\sqrt{\sigma^2{}_{h_i}{}^k + \sigma^2{}_{h_\xi}{}^k}} \leq Z^{a/2} \quad (1)$$

Where h_i^k, h_i^j, the estimated heights of an arbitrary point i for two successive years j and k, $\sigma^2{}_{h}{}^k{}_i$, $\sigma^2{}_{h}{}^k{}_\xi$ the estimated variances of the aforementioned heights and $z^{a/2}$ the value of the normal distribution, for a particular level of significance a. A level of confidence a = 0.05, thus $z^{a/2}$ = 1.96 was chosen. If equation (1) is fulfilled, the estimated displacement between two successive years is statistically insignificant. On the other hand, the failure of the test leads to the conclusion that the displacement and the uncertainty can be separated, meaning that the displacement can be measured with adequate confidence.

4. Results

4.1 Leveling measurements for the period 2018–2019

The leveling results between June 2018 and June 2019 are presented in Fig. 7. Starting from the reference point (S11), negative displacement on the z axis is increasing towards the SW side of the area of interest. This negative displacement indicates subsidence for every point of the dataset. Maximum subsidence value for this period is 15.1 ± 0.75 mm (S7), minimum is 2.9 ± 0.58 mm (S13) (Table 3). Therefore, for 2018–2019, only subsidence phenomena were observed over the study area.

4.2 Leveling measurements for the period 2019-2020

In this second set of results between June 2019 and June 2020, deformation seems to have a lower homogeneity (Fig. 8). More specifically, a significant number of points (5 out of 11) display values that are close to zero. These points are S1, S4, S6, S9, S10 and they are located in the middle of the area of interest, creating a cluster. Three out of eleven points seem to have an uplift trend. These points are S7, S13 and S14. The two

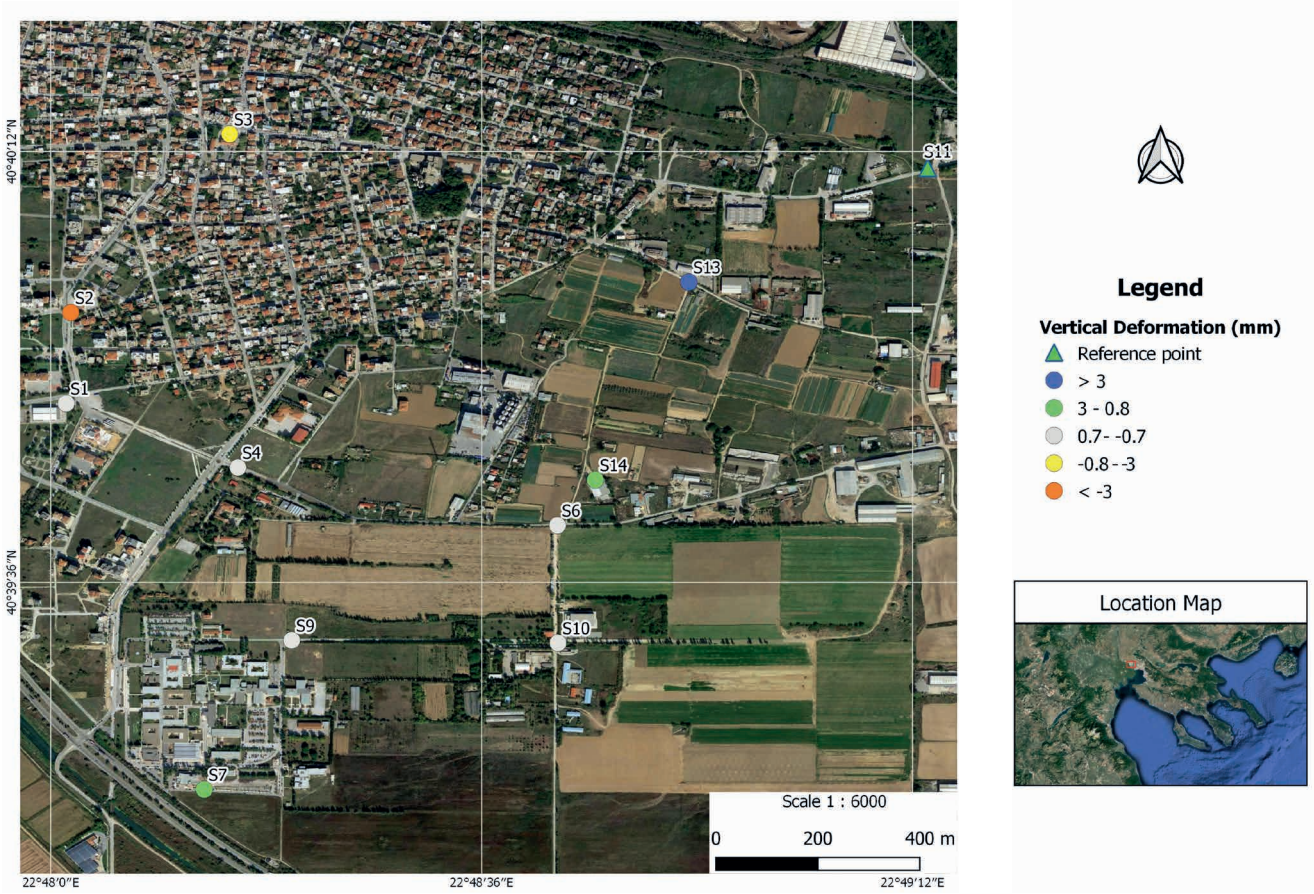

Fig. 8 Vertical displacements between June 2019 and June 2020.

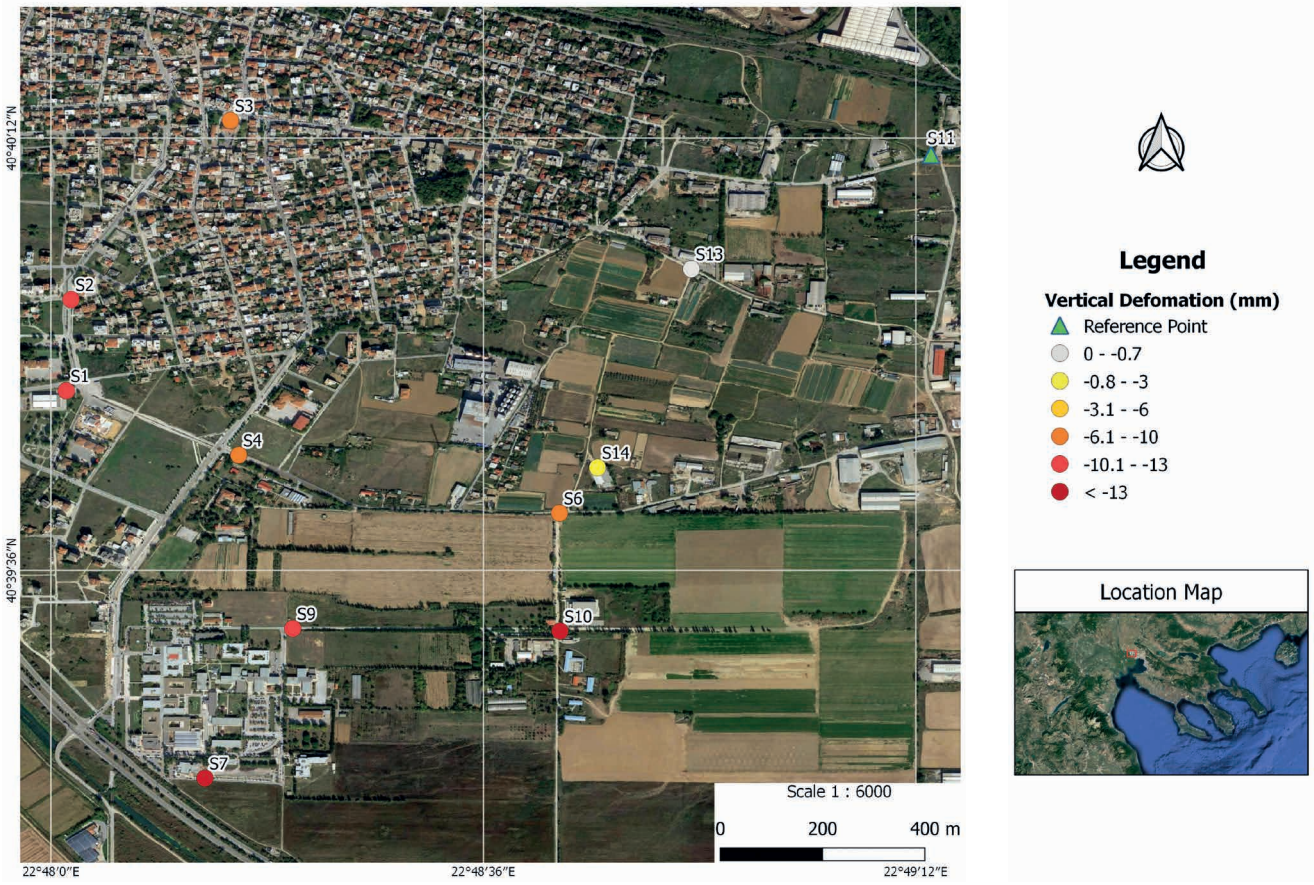

Fig. 9 Cumulative vertical displacements for the total study period (June 2018 – June 2020).

remaining points S2 and S3 seem to have a negative displacement (subsidence). Maximum subsidence value for this period is 3.4 ± 0.74 mm, while maximum uplift is 3.2 ± 0.57 mm (Tab. 3). Hence, in 2019–2020, both subsidence and uplift phenomena took place, but most of the points measured seem to be relatively stable.

4.3 Leveling measurements for the period 2018-2020

The third set of the measurements refers to the total difference between June 2018 and June 2020 (Fig. 9). One out of eleven points (S13), displays values that are close to zero, therefore it can be considered as overall stable. All other points of this dataset seem to have negative displacement (subsidence), which increases towards the SE part of the area. Maximum subsidence value for this period (which includes the total time range of the measurements) is 15.0 ± 0.71 mm (S10), minimum is 2.5 ± 0.67 mm (S14) (Tab. 3). In light of an overall interpretation, only subsidence phenomena appear to have taken place in the study area in this time frame. In this context, for a better overview of the ensemble deformation, a continuous surface was created by using the IDW (Inverse Distance Weighting) method.

Tab. 3 Summary of vertical deformation for every point of the established network, during each period of measurements. Subsidence/uplift are presented with negative/positive values respectively.

Loop	Loop closure 2018 (mm)	Loop closure 2019 (mm)	Loop closure 2020 (mm)
S3-S11-S13-S3		−0.2	0.5
S2-S13-S3-S2	−0.6	0.6	0.3
S1-S2-S13-S4-S1	−0.7	−0.2	−0.7
S4-S13-S14-S6-S4	0.5	−0.4	−0.4
S1-S4-S9-S1	0.2	−0.1	0.4
S1-S9-S7-S1	−0.4	0.3	0.6
S9-S4-S6-S9	−0.5	−0.4	0.3
S9-10-S6-S9	−0.2	0.1	−0.5
S7-S9-S10-S7	0.1	−0.3	−0.1

4.4 Control and Quality Analysis

The final closures for all measured loops, in accordance to Fig. 6, are presented, for each year, in Tab. 4.

Concerning quality analysis, all tests (according to Eq. 1) for the period 2018–2019 indicate statistically significant displacements. Conversely, for the period 2019–2020 half of the displacements identified

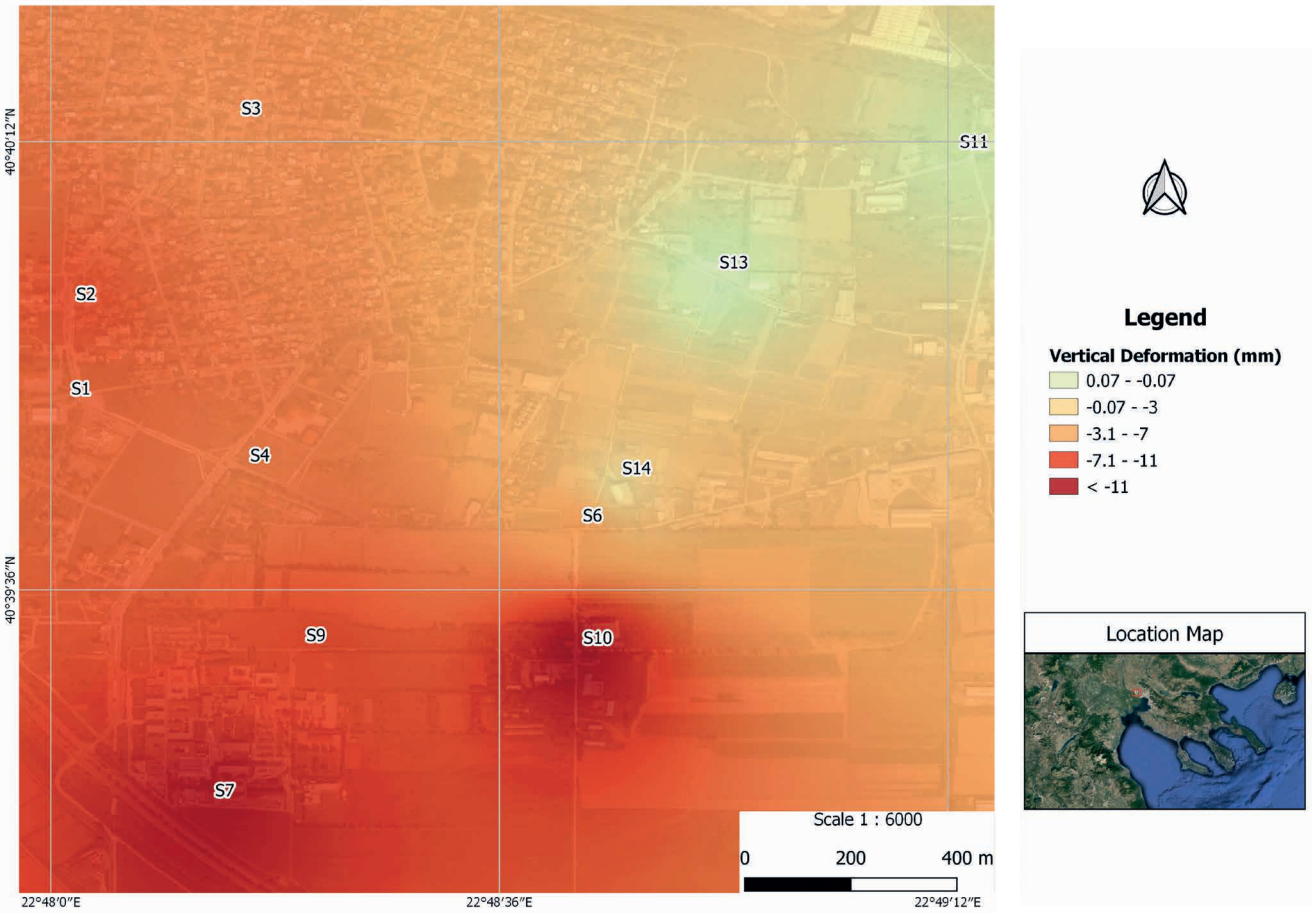

Fig. 10 Continuous surface of deformation for the period between 2018 to 2020, created by taking into account all eleven points of the dataset. This raster map is solely for visualization and qualitative interpretation purposes, hence the estimated values of deformation per pixel are indicative. As such, the map highlights an increasing subsidence towards the SW of the study area.

are statistically insignificant (S1, S4, S6, S9 and S10), while the total displacements between 2018–2020 are considered significant for all points except for S13.

After applying Least Squares (LS) adjustment, the accuracy (StD of the adjusted heights) ranged between 0.57 mm and 0.75 mm, with a mean value of about 0.7 mm.

Tab. 4 Loop closures for the 2018, 2019 and 2020 measurements.

Loop	Loop closure 2018 (mm)	Loop closure 2019 (mm)	Loop closure 2020 (mm)
S3-S11-S13-S3	0.4	−0.2	0.5
S2-S13-S3-S2	−0.6	0.6	0.3
S1-S2-S13-S4-S1	−0.7	−0.2	−0.7
S4-S13-S14-S6-S4	0.5	−0.4	−0.4
S1-S4-S9-S1	0.2	−0.1	0.4
S1-S9-S7-S1	−0.4	0.3	0.6
S9-S4-S6-S9	−0.5	−0.4	0.3
S9-10-S6-S9	−0.2	0.1	−0.5
S7-S9-S10-S7	0.1	−0.3	−0.1

5. Discussion

The three annual sets of high precision leveling measurements over the Sindos region have yielded reliable data – well below the mm level –, in order to ascertain the subtle vertical deformations occurring in the area.

The first set of measurements refers to the period between June 2018 and June 2019. For this timeframe, the displacement results over the ensemble network are negative, indicating a subsidence trend varying from 2.9 mm to 15.1 mm. Subsidence values seems to increase towards the SW part of the study area, i.e., to the south of Sindos and, in particular, in and around the facilities of the International Hellenic University (points S7 and S9). This increase of subsidence rate has been previously identified by several studies (Bolt et al. 1977; Mouratidis, Briole, and Ilieva 2010).

In the second dataset, for the period between June 2019 and June 2020, both negative (subsidence) and positive (uplift) deformation values have been recorded. Nevertheless, all of these values are much lower than those of 2018–2019, while five (i.e., almost 50%) of the measured points were determined to be stable. More specifically, points S1, S4, S6, S9 and S10, located at the center and towards the south of the study area, seem to be stable (deformation rate less then ± 0.7 mm). At the NW part of the study area, which also coincides with the denser urban environment of Sindos Town, negative values are recorded (points S2 and S3). The magnitude of subsidence over these two points is 2.9 mm and 3.4 mm respectively, for this second period of measurements. Finally, in the E–NE (S13 and S14) and far SW (S7) part of the study area, some positive displacement values have been measured. These correspond to an uplift of 3.2 mm, 3.0 mm and 0.8 mm, respectively. Taking into account the adjusted network accuracy of 0.7 mm, the uplift of S7 can be considered as marginally discernible. Given the geographic distribution of deformation during 2019–2020, S7 could be eventually considered as stable, given that all its nearest neighbors (S1, S4, S6, S9 and S10) are the points previously identified as stable as well.

Overall, during the full measurement timeframe, i.e., between June 2018 and June 2020, subsidence phenomena prevail over the whole study area, apart from one of the network points (S13), which is considered as stable, while no uplift signals have been recorded. The pattern of subsidence for these two years, is similar to the results for 2018–2019, i.e., values are maximized towards the S–SW (14.3 mm for S7 and 15.0 mm for S15).

As is evident from the individual (annual) results, a considerable difference in the deformation was identified between the two epochs (2018–2019 vs 2019–2020). In particular, the first year of measurements indicates clear subsidence (up to about 15 mm), whereas the second year is characterized by rather stable or significantly less perceptible displacements – whether uplift or subsidence – of about ± 3 mm. One possible explanation for these annual (or seasonal) differences may lie in the fact that changes of the aquifer level is followed by a proportional response detected at the surface (Raspini et al. 2014) and that sediments in the area are strongly affected by the underground water level (Raspini et al. 2014). These formations cover the majority of the study area and are indicative of high erosion and leaching. They are characterized by moderate to high permeability, frequently creating dynamic aquifers with evident water-level fluctuations. Additionally, according to (IGME 1993), phenomena of subsidence and soil displacement are observed as the direct result of urban expansion over these extensive sediment surfaces.

In order to investigate the correlation of subsidence trends with the aquifer level, aquifer level data over the study area was retrieved from the Thessaloniki Water Supply & Sewerage Company (EYATH S.A.). The data cover the period just before and right after the leveling measurements on a bi-annual basis from 2018 to 2020. The average aquifer level difference of all available borehole data, with reference to June 2018 – hence just before the start of the leveling campaigns – is presented in Fig. 11.

As it can be observed, the water level drops by more than 1m from June 2018 to May 2019 which is consistent to the observed clear subsidence during the same period. Conversely, during May 2019 – June 2020 the aquifer levels rise by about 0.35 m, which is again consistent with the more balanced behavior of the deformation phenomena in this time frame. Overall, the trend in the aquifer level changes

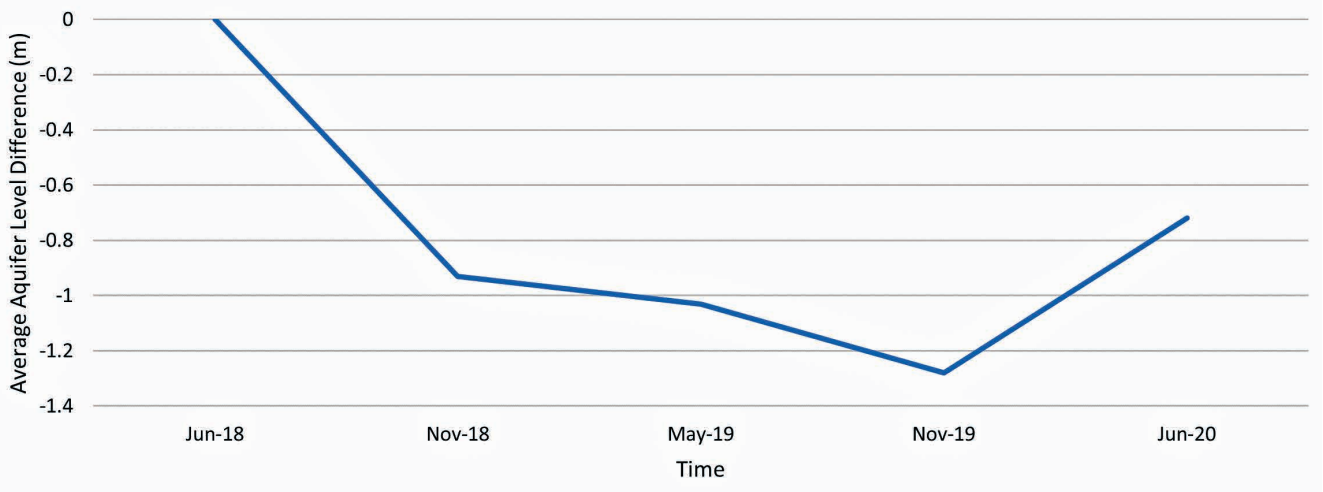

Fig. 11 Evolution of aquifer levels in the study area, during the period of the leveling measurements. All differences are presented with reference to June 2018 (source: EYATH S.A.).

resembles the pattern of the deformation phenomena, taking into account the time-lag between aquifer recharge and ground uplift mentioned in (Svigkas et al. 2016).

Additionally, monthly precipitation data of Sindos weather station were retrieved for the period 2018–2020 (apart from February 2020, for which the data were missing) (Meteo 2021). Subsequently, the total precipitation for the two individual time frames (June 2018 – May 2019 and June 2019 – May 2020) were calculated, yielding 342 mm and 528 mm respectively. This means that the precipitation of 2019–2020 was at least 54% more than that of 2018–2019, which may have slowed down or even partially reverted the subsidence phenomena for the specific year. Also, by retrieving all additional precipitation data from the Sindos weather station for previous years, dating back up to June 2015, the resulting average precipitation per year (June to May) is 420 mm. Interestingly enough, the minimum value (342 mm) is observed during the period between June 2018 – May 2019, i.e. coinciding with the clear subsidence trend measured; while the maximum value (528 mm) occurs between June 2019 – May 2020, i.e. coinciding with the more balanced deformation pattern identified in this period (Meteo 2021).

Compared to previous studies, which verified an ongoing decrease in the maximum subsidence rate per year, throughout the last three decades (Costantini et al. 2016), the current situation in Sindos seems to be following the same pattern. In particular, the rate of subsidence in the area continues to decline, from about 45 mm/yr in the period 1992–2001 (Raspini et al. 2014; Raucoules et al. 2008) and 34 mm/yr during 1993–2000 (Svigkas et al. 2016), to approximately 18 mm/yr during 2002–2007 (Mouratidis, Briole, and Ilieva 2010; Mouratidis et al. 2010) and 14 mm/yr for the period 2004–2010 (Costantini et al. 2016), to 10 mm/yr during 2014–2019 (Elias et al. 2020) and 14 mm/yr for 2015–2019 (Svigkas et al. 2020) and finally to about 7 mm/yr during 2018–2020 (from the results of this study). In contrast to this pattern, Svigkas et al. (Svigkas et al. 2016) reported an uplifting trend of about 12 mm/yr, for the period between 2003–2010 (Tab. 5 and Fig. 12). Note that all other studies were applied in broader area of Northern Greece, Thessaloniki region or specifically in Kalochori and Sindos regions. All the above-mentioned studies were based on InSAR methods (such as individual interferograms generation, Persistent Scatterer Interferometry and Small Baseline Subset approaches), hence, where appropriate, their results had to be converted from Line of Sight (LoS) deformation to vertical displacement (subsidence), in order to be comparable with the results of the current study.

Tab. 5 Rate of deformation in the broader area of Sindos based on all available relevant results.

Studies	Time Interval	Deformation Rate (mm/yr)
Raspini, F. et al. (2014), Raucoules, D. et al. (2008)	1992–2001	−45
Svigkas, N. et al. (2016)	1993–2000	−34
Mouratidis, A. et al. (2010)	2002–2007	−18
Costantini, F. et al. (2016)	2004–2010	−14
Svigkas, N. et al. (2020)	2003–2010	12
Elias, P. et al. (2020)	2014–2019	−10
This study	2018–2020	−7

The main limitation of this study lies in the restrictions related to the distance that can be covered by leveling, in order to ensure that the reference point is clearly outside the deforming area, thus stable with respect to the other network points. Pre-existing information and literature as well as achieved results converge that S11 lies at the farthermost end of the least affected-by ground deformation-area. Thus, S11 was by evidence the optimum choice for a reference point for the purposes of this study.

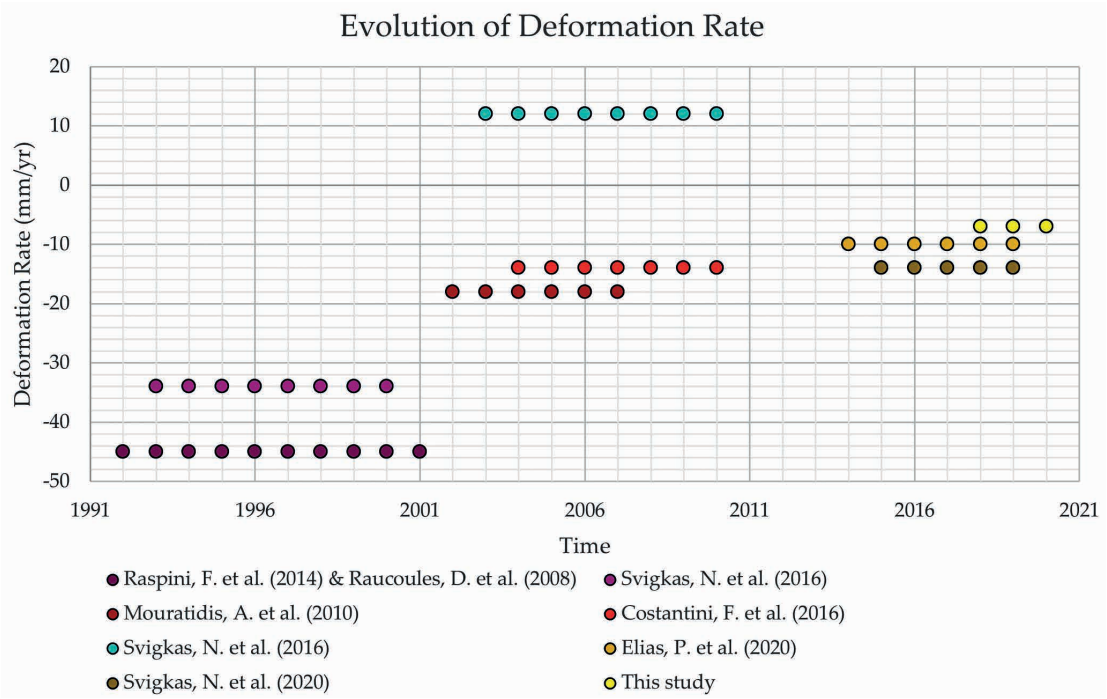

Fig. 12 Graphical representation of the evolution of the rate of deformation throughout the years in the broader area of Sindos region.

6. Conclusions

In this study, subtle vertical motions in the Sindos region, Thessaloniki, northern Greece, were measured three times, in three consecutive years (June of 2018, 2019 and 2020), by creating a high precision leveling network of eleven points over an area of about 5 km^2. Measured also with GNSS, this network comprises a scientific "investment" for the continual observation of vertical deformation in the study area, in the coming years or decades.

The first pair of measurements (June 2018 – June 2019) reveals considerable subsidence over the whole study area, while the second period (June 2019 – June 2020) is predominantly characterized by relative stability or significantly lower deformation – subsidence or uplift – values. Over the full two-year period (2018–2020), the area is clearly dominated by a subsidence trend, with a total maximum value of up to 15.0 mm. Although this value corresponds to a subsidence rate of about 8 mm/yr, special attention ought to be given to the non-linear nature of the phenomena involved, as verified by the year-to-year measurements. This phenomenon can be, by hard evidence, attributed to the different amounts of annual precipitation, the intensity of ground water exploitation and the consequent variations of the aquifer level.

The identified on-going subsidence at progressively lower rate is particularly evident and in line with the vast majority of previous relevant studies of the last three decades.

Overall, it is acknowledged that the current study investigates only a "temporal window" of a diachronic and dynamic phenomenon of deformation that has been quantitatively studied via reliable ground- and satellite-based methods (leveling, GNSS, InSAR) for more than three decades. As such, but also due to the considerable decrease of the subsidence rate and the consequent reduction of the signal/noise ratio during the last 10–15 years, it has been considered imperative to scale-up the precision of observations.

High precision leveling over such an extensive area requires a lot of properly trained human resources and engineering expertise, is very time-consuming, costly and tedious. Nevertheless, the resulting output was rather essential, in order to constrain and be able to map and monitor the current subtle deformation signal manifestations in the study area.

Apart from resolving the ambiguity of downward/upward displacements and the indication of non-linear deformation patterns, the established network and measurements shall serve as a basis for future monitoring. Additionally, they also constitute invaluable assets for the validation of alternative/complementary geodetic methods, such as those of GNSS and InSAR, or the synergistic use of all three approaches simultaneously. In fact, the study area has been monitored since 1991, almost continuously, with InSAR (apart from 2011–2013, due to the lack of SAR data), while the subsidence phenomena have been evolving. Thus, the leveling network as well as the GNSS measurements (to be periodically repeated in the future) will render this case study as an ideal test site for the cross validation of geodetic methods (InSAR, GNSS, leveling) and/or the optimization of their combined use. This is e.g., expected to contribute to the overall deterioration of opportunistic InSAR results (Hanssen 2003) and to overcoming the limitations of the individual geodetic methods.

In this context, it is of high scientific value that the research expands in space and time, in order to have a clear representation and understanding of the phenomenon and its progress throughout the years, as well as to ascertain the potential periodicity of ground deformation.

Acknowledgements

The authors would like to thank the Thessaloniki Water Supply & Sewerage Company (EYATH S.A.) for providing access to hydrological data and especially Thomas Spachos for his availability and cooperation.

References

Amighpey, M., Behzad, V., Arabi, S. (2016): Modeling Interseismic Deformation Field of North Tehran Fault Extracted from Precise Leveling Observation. Tectonophysics 679, 169–179, https://doi.org/10.1016/j.tecto.2016.04.051.

Andronopoulos, B., Rozos, D., Hadzinakos, I. (1991): Subsidence Phenomena in the Industrial Area of Thessaloniki, Greece. International Association of Hydrological Sciences 200, 59–69, https://doi.org/10.1016/0148-9062(92)92181-B.

Argyrakis, P., Ganas, A., Valkaniotis, S. et al. (2020): Anthropogenically induced subsidence in Thessaly, central Greece: new evidence from GNSS data. Natural Hazards 102(1), 179–200, https://doi.org/10.1007/s11069-020-03917-w.

Astaras, T. A., Sotiriadis, L. (1988): The Evolution of the Thessaloniki-Giannitsa Plain in Northern Greece during the Last 2500 Years: From the Alexander the Great Era until Today. In INQUA/IGCP 158 Meeting on the Palaeohydrological Changes during the Last 15 000 Years, 105–114.

Delgado Blasco, J. M., Foumelis, M., Stewart, C., Hooper, A. (2019): Measuring Urban Subsidence in the Rome Metropolitan Area (Italy) with Sentinel-1 SNAP-StaMPS Persistent Scatterer Interferometry. Remote Sensing 11(2), 1–17, https://doi.org/10.3390/rs11020129.

Bolt, B. A., Horn, W. L., Macdonald, G. A., Scott, R. F. (1977): Hazards from Ground Subsidence. In Geological Hazards, 198–220. Springer Study Edition. Springer, New York, NY, https://doi.org/10.1007/978-1-4615-7101-8_5.

Chen, H.-Y., Lee, J.-Ch., Tung, H., Chen, Ch.-L., Lee, H. (2021): Variable Vertical Movements and Their Deformation Behaviors at Convergent Plate Suture: 14-Year-Long (2004–2018) Repeated Measurements of Precise Leveling around Middle Longitudinal Valley in Eastern Taiwan. Journal of Asian Earth Sciences 218, 104865, https://doi.org/10.1016/j.jseaes.2021.104865.

Costantini, F., Mouratidis, A., Schiavon, G., Sarti, F. (2016) Advanced InSAR Techniques for Deformation Studies and for Simulating the PS-Assisted Calibration Procedure of Sentinel-1 Data: Case Study from Thessaloniki (Greece), Based on the Envisat/ASAR Archive. International Journal of Remote Sensing 37(4), 729–744, https://doi.org/10.1080/01431161.2015.1134846.

Dermanis, A. (1986): Adjustments of the Observations and Estimation Theory. 2nd ed. Ziti Publications, Thessaloniki, Greece (in Greek).

Dermanis, A., Fotiou, A. (1992): Applications of the Adjustments of the Observations. Ziti Publications, Thessaloniki (in Greek).

Dermanis, A., Rossikopoulos, D. (1981): The DeRos Programm for the Adjustment of Large Triangulation Networks. Quartiones Geodesica 2, 191–203.

Dimopoulos, G., Stournaras, G., Pavlopoulos, K. (2005): Investigation of the Conditions Generating Soil Settlements in Sindos-Kalochori Area of Thessaloniki. In Proceedings of the 7th Hellenic Hydrogeological Conference and 2nd MEM Workshop on Fissured Rocks Hydrogeology 1, 135–146.

Doukakis, E. (2005): Coastal Red Spots along the Western Thermaikos Gulf. In Proceedings of the 9th International Conference on Environmental Science and Technology, Rhodes, Greece, University of Aegean, Rhodes, A334–A339.

Elias, P., Benekos, G., Perrou, T., Parcharidis, I. (2020): Spatio-Temporal Assessment of Land Deformation as a Factor Contributing to Relative Sea Level Rise in Coastal Urban and Natural Protected Areas Using Multi-Source Earth Observation Data. Remote Sensing 12(14), 2296, https://doi.org/10.3390/rs12142296.

Fryksten, J., Nilfouroushan, F. (2019): Analysis of Clay-Induced Land Subsidence in Uppsala City Using Sentinel-1 SAR Data and Precise Leveling. Remote Sensing 11(23), 2764, https://doi.org/10.3390/rs11232764.

Ghilardi, M., Fouache, E., Queyrel, F., Syrides, G., Vouvalidis, K., Kunesch, S., Styllas, M., Stiros, S. (2008): Human Occupation and Geomorphological Evolution of the Thessaloniki Plain (Greece) since Mid Holocene. Journal of Archaeological Science 35(1), 111–125, https://doi.org/10.1016/j.jas.2007.02.017.

Guanming, G., Hui, X., Ronhui, L., Feng, H. (2019): Research on Construction Control Network Technology of Hydropower Project in Steep Mountainous Area. IOP Conference Series: Earth and Environmental Science 371(2), 022095, https://doi.org/10.1088/1755-1315/371/2/022095.

Hadzinakos, I., Rozos, D., Apostolidis, E. (1990): Engineering Geological Mapping and Related Geotechnical Problems. In International Congress International Association of Engineering Geology 6, 127–134

Hanssen, R. (2003): Haphazard Occurrences of Reality: The Link between Opportunism, Geodesy, and Satellite Radar Interferometry. Guy Bamford Lecture. 2003. Available online: https://citeseerx.ist.psu.edu/viewdoc/download?doi=10.1.1.590.4384&rep=rep1&type=pdf (accessed: 2. 10. 2022).

Hao, M., Wang, Q., Shen, Z., Cui, D., Ji, L., Li, Y., Qin, S. (2014): Present Day Crustal Vertical Movement Inferred from Precise Leveling Data in Eastern Margin of Tibetan Plateau. Tectonophysics 632, 281–292, https://doi.org/10.1016/j.tecto.2014.06.016.

Hung, W.-C., Hwang, C., Chen, Y.-A., Zhang, L., Chen, K.-H., Wei, S.-H., Huang, D.-R., Lin, S.-H. (2018): Land Subsidence in Chiayi, Taiwan, from Compaction Well, Leveling and Alos/Palsar: Aquaculture-Induced Relative Sea Level Rise. Remote Sensing 10(1), 40, https://doi.org/10.3390/rs10010040.

IGME (1993): Engineering Geological Map of Greece, Scale 1 : 500,000. Institute of Geology and Mineral Exploration, Athens.

Kall, T., Oja, T., Tänavsuu, K. (2014): Postglacial Land Uplift in Estonia Based on Four Precise Levelings. Tectonophysics 610, 25–38, https://doi.org/10.1016/j.tecto.2013.10.002.

Koch, K. R. (1999): Parameter Estimation and Hypothesis Testing in Linear Models. 2nd ed. Springer Berlin, Heidelberg, https://doi.org/10.1007/978-3-662-03976-2.

Mattas, C., Voudouris, K. S., Panagopoulos, A. (2014): Integrated Groundwater Resources Management Using the DPSIR Approach in a GIS Environment: A Case Study from the Gallikos River Basin, North Greece. Water 6(4), 1043–1068, https://doi.org/10.3390/w6041043.

Meteo (2021): Percipitation Data. Meteo. 2021. Available online: http://meteosearch.meteo.gr/ (accessed: 5. 10. 2022).

Mouratidis, A. (2017): Contribution of GPS and GIS Assisted Spaceborne Remote Sensing in the Morphotectonic Research of Central Macedonia (Northern Greece), Aristotle University of Thessaloniki: Thessaloniki, Greece.

Mouratidis, A., Astaras, T., Pavlidis, S., Tsakiri, M., Ilieva, M., Rolandone, F. (2010): Contribution of InSAR and Kinematic GPS Data to Subsidence and Geohazard Monitoring in Central Macedonia (N. Greece). In Proceedings of the XIX CBGA Congress, Thessaloniki, Greece, 100, 535–545.

Mouratidis, A., Briole, P., Ilieva, M., Astaras, T., Rolandone, F., Baccouche, M. (2010): Subsidence and Deformation Phenomena in the Vicinity of Thessaloniki (N. Greece) Monitored by Envisat/Asar Interferometry. Proceedings of Fringe 2009: Advances in the Science and Applications of SAR Interferometry at: Frascati, Italy, ESA SP-677.

Mouratidis, A., Costantini, F., Votsis, A. (2011): Correlation of DInSAR Deformation Results and Active Tectonics in the City of Thessaloniki (Greece). 2011 Joint Urban Remote Sensing Event, JURSE 2011 – Proceedings, 421–424, https://doi.org/10.1109/JURSE.2011.5764809.

Nicholls, R. J., Lincke, D., Hinkel, J. et al. (2021): A Global Analysis of Subsidence, Relative Sea-Level Change and Coastal Flood Exposure. Nature Climate Change 11(4), 338–342, https://doi.org/10.1038/s41558-021-00993-z.

Pateli, M., Krigas, N., Karousou, R., Hanlidou, E., Kokkini, S. (2002): Vascular Plants in Thc Suburban Arca or Thessaloniki (N Grecce). I. Thc Industriai Park or Sindos. Flora Mediterranea 12, 323–339.

Psimoulis, P., Ghilardi, M., Fouache, E., Stiros, S. (2007): Subsidence and Evolution of the Thessaloniki Plain, Greece, Based on Historical Leveling and GPS Data. Engineering Geology 90(1–2), 55–70, https://doi.org/10.1016/j.enggeo.2006.12.001.

Raspini, F., Loupasakis, C., Rozos, D., Adam, N., Moretti, S. (2014): Ground Subsidence Phenomena in the Delta Municipality Region (Northern Greece): Geotechnical Modeling and Validation with Persistent Scatterer Interferometry. International Journal of Applied Earth Observation and Geoinformation 28(1), 78–89, https://doi.org/10.1016/j.jag.2013.11.010.

Raucoules, D., Parcharidis, I., Feurer, D., Novalli, F., Ferretti, A., Carnec, C., Lagios, E., Sakkas, V., Le Mouelic, S., Cooksley, G., and Hosford, S. (2008): Ground Deformation Detection of the Greater Area of Thessaloniki (Northern Greece) Using Radar Interferometry Techniques. Natural Hazards and Earth System Science 8(4), 779–788, https://doi.org/10.5194/nhess-8-779-2008.

Rossikopoulos, D. (1999). Surveying Networks and Computations. 2nd ed. Ziti Publications, Thessaloniki (in Greek).

Rozos, D., Apostolidis, E., Xatzinakos, I. (2004): Engineering-Geological Map of the Wider Thessaloniki Area, Greece. Bulletin of Engineering Geology and the Environment 63(2), 103–108, https://doi.org/10.1007/s10064-004-0237-6.

Del Soldato, M., Farolfi, G., Rosi, A., Raspini, F., Casagli, N. (2018): Subsidence Evolution of the Firenze-Prato-Pistoia Plain (Central Italy) Combining PSI and GNSS Data. Remote Sensing 10(7), 1–19, https://doi.org/10.3390/rs10071146.

Stiros, S.C. (2001): Subsidence of the Thessaloniki (Northern Greece) Coastal Plain, 1960-1999. Engineering Geology 61(4), 243–56, https://doi.org/10.1016/S0013-7952(01)00027-8.

Svigkas, N., Loupasakis, C., Papoutsis, I., Kontoes, C., Alatza, S., Tzampoglou, P., Tolomei, C., Spachos, T. (2020): InSAR Campaign Reveals Ongoing Displacement Trends at High Impact Sites of Thessaloniki and Chalkidiki, Greece. Remote Sensing 12, 2396, https://doi.org/10.3390/rs12152396.

Svigkas, Nikos, Papoutsis, I., Loupasakis, C., Tsangaratos, P., Kiratzi, A., Kontoes, C. (2016): Land Subsidence Rebound Detected via Multi-Temporal InSAR and Ground Truth Data in Kalochori and Sindos Regions, Northern Greece. Engineering Geology 209, 175–186, https://doi.org/10.1016/j.enggeo.2016.05.017.

Tsourlos, P., Vargemezis, G., Voudouris, C., Spachos, T., Stampolidis, A. (2007): Monitoring Recycled Water Injection into a Confined Aquifer in Sindos (Thessaloniki) Using Electrical Resistivity Tomography (ERT): Installation and Preliminary Results. Bulletin of the Geological Society of Greece 40(2), 580–592, https://doi.org/10.12681/bgsg.16333.

USGS (2021): Spirit Leveling. United States Geological Survey. Available online: https://www.usgs.gov/centers/ca-water-ls/science/spirit-leveling?qt-science_center_objects=0#qt-science_center_objects (accessed: 17. 5. 2021).